Bundle-forming pilus retraction enhances enteropathogenic *Escherichia coli* infectivity

Eitan E. Zahavi[a], Joshua A. Lieberman[b], Michael S. Donnenberg[b], Mor Nitzan[c], Kobi Baruch[d], Ilan Rosenshine[d], Jerrold R. Turner[e], Naomi Melamed-Book[f], Naomi Feinstein[f], Efrat Zlotkin-Rivkin[a], and Benjamin Aroeti[a]

[a]Department of Cell and Developmental Biology, Institute of Life Sciences, Hebrew University of Jerusalem, Jerusalem 91904, Israel; [b]Division of Infectious Diseases, University of Maryland School of Medicine, Baltimore, MD 21201; [c]Racah Institute of Physics, Hebrew University of Jerusalem, Jerusalem 91904, Israel; [d]Department of Microbiology and Molecular Genetics, IMRIC, Hadassah-Hebrew University Medical School, Hebrew University, Jerusalem, Israel; [e]Department of Pathology, University of Chicago, Chicago, IL 60637; [f]Bioimaging Unit, Institute of Life Sciences, Hebrew University of Jerusalem, Jerusalem 91904, Israel

ABSTRACT **Enteropathogenic *Escherichia coli* (EPEC) is an important human pathogen that causes acute infantile diarrhea. The type IV bundle-forming pili (BFP) of typical EPEC strains are dynamic fibrillar organelles that can extend out and retract into the bacterium. The *bfpF* gene encodes for BfpF, a protein that promotes pili retraction. The BFP are involved in bacterial autoaggregation and in mediating the initial adherence of the bacterium with its host cell. Importantly, BFP retraction is implicated in virulence in experimental human infection. How pili retraction contributes to EPEC pathogenesis at the cellular level remains largely obscure, however. In this study, an effort has been made to address this question using engineered EPEC strains with induced BFP retraction capacity. We show that the retraction is important for tight-junction disruption and, to a lesser extent, actin-rich pedestal formation by promoting efficient translocation of bacterial protein effectors into the host cells. A model is proposed whereby BFP retraction permits closer apposition between the bacterial and the host cell surfaces, thus enabling timely and effective introduction of bacterial effectors into the host cell via the type III secretion apparatus. Our studies hence suggest novel insights into the involvement of pili retraction in EPEC pathogenesis.**

Monitoring Editor
Keith E. Mostov
University of California, San Francisco

Received: Jan 3, 2011
Revised: Apr 14, 2011
Accepted: May 18, 2011

INTRODUCTION

Enteropathogenic *Escherichia coli* (EPEC) is a major cause of acute infantile diarrhea mainly in developing countries (Taylor and Echeverria, 1993; Nataro and Kaper, 1998; Chen and Frankel, 2005; Marcos and DuPont, 2007). Typical EPEC strains produce proteinaceous fibrillar organelles that extend out from the bacterial surface, known as bundle-forming pili (BFP), members of the type IV pili (Tfp) family. Tfp are expressed on the surface of a variety of other Gram-negative (e.g., *Neisseria gonorrhea*, *Neisseria meningitidis*, and *Pseudomonas aeruginosa*), as well as in Gram-positive (e.g., *Clostridium perfringens*) pathogenic bacteria. Ample evidence suggests that the Tfp, including those of EPEC, are important virulence factors. In addition to their role in facilitating the initial attachment of the microbe to its host cell surface (Milgotina, 2009), they promote cytoskeletal rearrangements and elicit signaling events that assist the microbe to adopt an extracellular lifestyle (Kline *et al.*, 2009; Boettcher *et al.*, 2010). The ways by which Tfp influence their host cells are still poorly understood, however.

Typical EPEC strains harbor a ~95 kb EPEC adherence factor plasmid containing an operon of 14 genes encoding for complete and functional BFP (Donnenberg *et al.*, 1992; Giron *et al.*, 1993; Iguchi *et al.*, 2009). BFP are postulated to initiate a long-range adhesion of bacteria with the intestinal epithelium. In addition, BFP recruit

This article was published online ahead of print in MBoC in Press (http://www.molbiolcell.org/cgi/doi/10.1091/mbc.E11-01-0001) on May 25, 2011.

Address correspondence to: Benjamin Aroeti (aroeti@cc.huji.ac.il).

Abbreviations used: BFP, the type IV bundle-forming pili; BlaM, β-lactamase; EPEC, enteropathogenic *Escherichia coli*; FCS, fetal calf serum; FITC, fluorescein isothiocyanate; LEE, locus of enterocyte effacement; mRFP, monomeric red fluorescent protein; PBS, phosphate-buffered saline; PI, phosphoinositide; PM, plasma membrane; PY-Tir, tyrosine-phosphorylated Tir; TER, *trans*-epithelial electrical resistance; T3SS, type III secretion system; Tfp, type IV pili; Tir, translocated intimin receptor; TJs, tight junctions.

other EPEC cells into aggregates; this recruitment results in the presence of bacterial microcolonies on the cell surface, a phenomenon called localized adherence. Bacterial aggregation can also occur in tissue culture medium. This process, which is termed autoaggregation, has been hypothesized to be mediated by the extension of the pilus fiber due to biogenesis and subsequent oligomerization of its pilin subunits (i.e., bundlin encoded by *bfpA*). Bacterial aggregates can disaggregate and disperse. The dispersion phenotype is facilitated by the retraction of the pilus fiber, owing to dissociation of pilin subunits and their degradation (Humphries *et al.*, 2010). Two genes encoding BfpD and BfpF (putative ATPases) drive pilus extension and retraction, respectively. Disruption of any of these genes leads to anomalies in BFP functions. For instance, a *bfpF* mutant is hyperpilated, and forms bacterial aggregates that fail to disperse over time. A *bfpD* mutant does not express BFP, does not autoaggregate, and is deficient in localized adherence phenotype.

BFP is a crucial virulence factor (see next section), and as such should be regarded in the broader context of EPEC pathogenesis. The EPEC-induced disease is characterized by at least four histopathological hallmarks: 1) intimate adherence of the microbe to epithelial cells of the small intestine; 2) the loss of absorptive microvili (effacement); 3) formation of actin-rich pedestals beneath the adherent bacteria; and 4) loss of tight junctions (TJs). It is clear that these phenotypes largely depend on the expression of proteins encoded by genes harbored within the chromosomal locus of enterocyte effacement (LEE). In particular, the association between two LEE proteins–intimin, which resides in the bacterial surface, and the translocated intimin receptor (Tir), which is translocated into the host cell plasma membrane (PM) by the type III secretion system (T3SS)–has been rigorously characterized. These molecular associations promote an intimate link between the bacterium and its host cell and the elicitation of signal transduction pathways, which lead to actin condensation and to the generation of actin-rich pedestals (Rothbaum *et al.*, 1982, 1983; Taylor *et al.*, 1986; Jerse *et al.*, 1990). Intimin-Tir association and translocation of additional T3SS protein effectors trigger complex signaling cascades that promote significant alterations in the actin cytoskeleton, the secretion of ions (e.g., Cl^- and HCO_3^-), mislocalization of aquaporins, and the disruption of epithelial TJs. The manipulation of these processes is believed to lead to tissue damage and the diarrheal effect (for a review, see Guttman and Finlay, 2009).

Experiments performed in humans have clearly suggested that the BFP is required for EPEC pathogenesis. In these experiments, volunteers ingested a range of inocula of wild type, *bfpA, bfpT (perA),* or *bfpF* mutant bacteria. Significantly fewer volunteers who ingested the mutant bacteria developed diarrhea, and elicitation of diarrhea required a 200-fold-higher bacterial dose in the *bfpF* mutant, relative to the wild- type strain (Bieber *et al.*, 1998). Although these data suggest that BFP and its retraction capacity are important virulence factors in vivo, the precise effects they have on host cells remain unknown. Here to investigate the effects of BFP retraction on epithelial host cells we used genetically engineered EPEC strains, which can retract their pili upon induction with arabinose. We found that BFP retraction contributes to timely and efficient export of bacterial protein effectors into the host cell, where they exert key functions in EPEC pathogenesis, including disruption of the epithelial barrier and generation of actin-rich pedestals.

RESULTS

BfpF is required for disruption of TJs

A common perception suggests that disruption of epithelial TJs' barrier functions by EPEC infection contributes to the diarrheal disease (Guttman and Finlay, 2008). Because BfpF has been implicated in the development of the disease (Bieber *et al.*, 1998), we reasoned that the bacterial protein may be involved in the breakdown of TJs. To test this hypothesis, the TJ barrier functions of EPEC infected and untreated MDCK cells were examined by simultaneous monitoring of the *trans*-epithelial electrical resistance (TER; Figure 1A, top panel) and cell monolayer permeability to 4 kDa fluorescein isothiocyanate (FITC)-dextran (Figure 1A, bottom panel). Infection with the T3SS defective EPEC-*escV* (*escV::Tn5kan*) or pilin-deficient EPEC-*bfpA* (*bfpA::TnphoA*), which is incapable of microcolony formation, resulted in an increase in TER values. In both cases, cell monolayer permeability to FITC-dextran penetration was minimal, nearly indistinguishable from untreated control cells. Cell infection with wild-type EPEC (EPEC-*wt*) caused a significant reduction in TER and a concomitant increase in permeability to dextran. Both these effects were particularly apparent after 4 h of infection. EPEC-*bfpA* has reduced capacity of host cell colonization (Donnenberg *et al.*, 1990; Hyland *et al.*, 2008), and marginal capability to inject bacterial effectors into the host cell (Mills *et al.*, 2008). We hence hypothesize that this change in TER reflects tightening of the epithelial junctions in response to bacteria that are either defective in T3SS or have poor cell colonization. The effect is probably counteracted by junctional disrupting protein effectors that are translocated into the host cells upon infection with EPEC-*wt*.

To further investigate the role of BFP dynamics in TJ disruption, we used a newly engineered EPEC strain, in which pili retraction is induced in response to arabinose (EPEC-*bfpF* +$BfpF^{ara}$; see *Materials and Methods*). Host cell colonization of this EPEC strain is similar to that of EPEC-*wt* (Figure 2B and Supplemental Figure S1), thus enabling specific examination of the effects of pili retraction on the host cell. Cell infection with EPEC-*bfpF* +$BfpF^{ara-}$ (i.e., BfpF expression is suppressed) prompted an increase in the TER values, albeit at a lower extent than that observed for EPEC-*escV*. Nevertheless, the levels of paracellular penetration of FITC-dextran recorded for this EPEC strain were similar to those of EPEC-*escV* or of untreated controls. In contrast, when cells were infected with the same strain in the presence of arabinose (EPEC-*bfpF* +$BfpF^{ara+(T0)}$; i.e., BfpF expression was induced), a significant drop in TER, which was apparent after 1 h of infection, and an increase in monolayer penetration of FITC-dextran were observed. Interestingly, an identical response was measured when cells were first infected with EPEC in the absence of arabinose for 2 h and then exposed to the inducer for the rest of the infection time (*bfpF* +$BfpF^{ara+(T2)}$). Taken together, these observations reinforce the notion that BfpF expression is required for TJ dysfunction induced by EPEC. Because BFP is involved in bacterial adherence, we quantified cell-associated bacteria after 4 h of infection (see Supplemental Figure S1). The results did not reveal significant differences between the various EPEC strains with respect to their capacity to adhere to the host cells. This finding suggests that the effects on the epithelial barrier functions were not due to gross differences in attachment to host cells.

EPEC naturally infects human enterocytes of the small intestine. Hence, similar experiments were conducted on the Caco-2BBe enterocytes (Hidalgo *et al.*, 1989; Supplemental Figure S2). Data were essentially similar to those obtained with MDCK cells. Addition of arabinose [*bfpF* +$BfpF^{ara+(T0)}$] stimulated both a decrease in TER and an increase in monolayer leakiness, showing levels similar to those observed for EPEC-*wt*. These results are once again consistent with the notion that BFP retraction contributes to the capacity of EPEC to disrupt the TJs.

TJ barrier dysfunction obtained upon EPEC infection correlates with the dissociation of junctional proteins, such as ZO-1

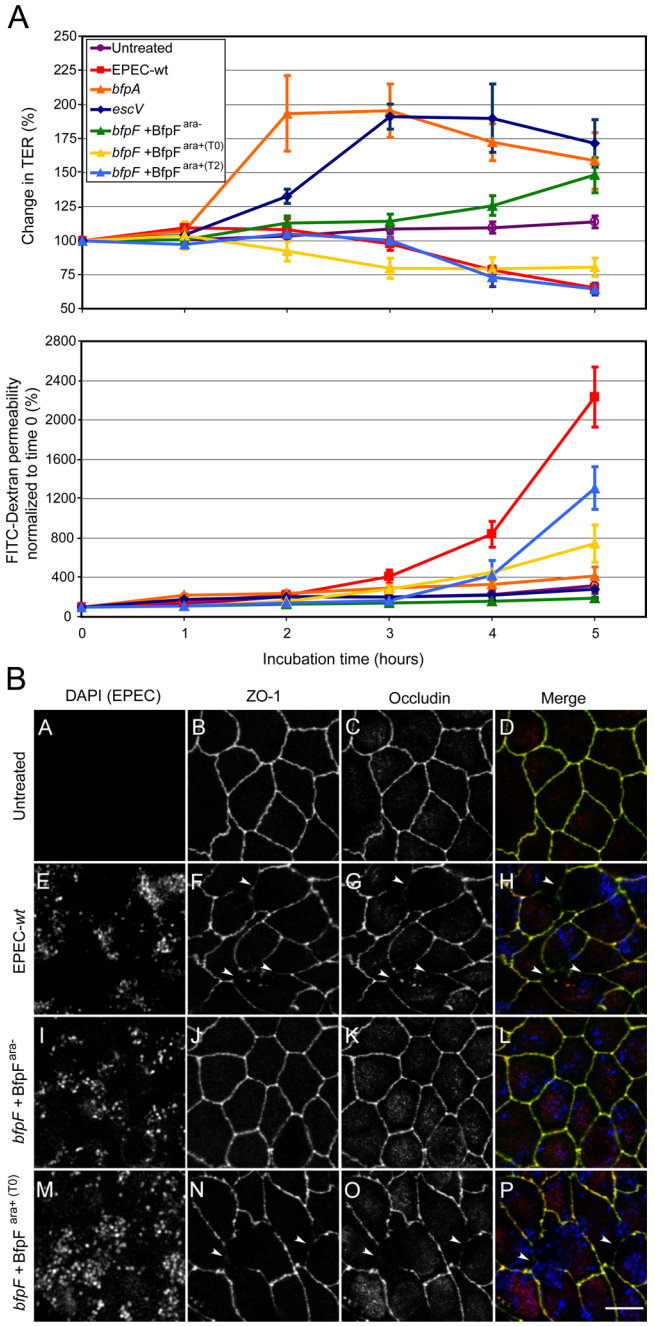

FIGURE 1: Induced BfpF expression perturbs the functions and morphology of TJs. MDCK cells cultured on semipermeable supports were infected with the indicated EPEC strains, or left untreated, as described in *Materials and Methods*. Infection with EPEC-*bfpF* +BfpF was performed in the absence (EPEC-*bfpF* +BfpF^{ara-}) or presence (EPEC-*bfpF* +BfpF^{ara+}) of arabinose. In some experiments, arabinose was added to the activation medium 15 min before cell infection and throughout the entire infection time (EPEC-*bfpF* +BfpF$^{ara+(T0)}$). In other experiments, cells were initially infected in the absence of arabinose for 2 h, and then arabinose was added to the infection medium for the rest of the infection time (EPEC-*bfpF* +BfpF$^{ara+(T2)}$). (A) Barrier functions. Changes in the TJ barrier functions were measured by tracking the alterations in TER (top panels) and monolayer permeability to FITC-dextran (bottom panels). Results are mean ± SE of at least three independent experiments, each of which was performed in duplicate. Data are normalized to values measured at time zero. Two-tailed Student's *t* test reveals that infection with EPEC expressing intact BfpF resulted in statistically significant reduction in TER and increase in cell monolayer permeability after 5 h of infection (see Table S4). (B) Junctional morphology. Polarized MDCK monolayers were infected with the indicated EPEC strains for 3 h at 37°C, or left untreated. Cells were then fixed and costained with DAPI (bacteria and nuclei), anti–ZO-1 and anti-occludin antibodies. Fluorescence labeling was analyzed by confocal microscopy. Images are projections of *x*–*y* sections, taken along 2–3 μm from the cell's apex, where bacteria and junctional labeling was best visualized. Arrowheads indicate examples of breaks in occludin and ZO-1 staining. Bar = 10 μm.

(Philpott *et al.*, 1996) and occludin (Simonovic *et al.*, 2000) from the cell periphery. We used indirect immunofluorescence and confocal microscopy to examine the distribution of these junctional proteins following EPEC infection (Figure 1B). Polarized MDCK monolayers were infected with EPEC-*wt*, EPEC-*bfpF* +BfpF^{ara-}, or EPEC-*bfpF* +BfpF$^{ara+(T0)}$ or were left untreated. Cells were then stained with DAPI (to visualize bacteria), and immunolabeled with anti-ZO-1 and anti-occludin antibodies. Confocal analyses showed the typical honeycomb-like and continuous staining of the cell-cell junctions in the most apical region of untreated cells, and of cells infected with EPEC-*bfpf* +BfpF^{ara-}. This pattern of staining became fragmented upon cell infection with EPEC-*wt* or EPEC-*bfpF* +BfpF$^{ara+(T0)}$, suggesting that BfpF expression is required for EPEC-mediated alterations in the TJ structure.

BfpF is essential for timely and effective translocation of EspF

EspF has been shown to play a central role in the disruption of epithelial TJ (McNamara *et al.*, 2001; Guttman *et al.*, 2006). We have similarly observed that the ability of EPEC to disrupt the TJ of MDCK cells is abolished upon infection with EPEC-Δ*espF* (E. Wircer, unpublished data). We hence reasoned that, upon infection with an EPEC strain carrying dysfunctional *bfpF*, delivery of EspF into the host cell is impaired, and consequently the capacity of EPEC to disrupt the TJ barrier is reduced. To test this hypothesis, we examined the involvement of BFP retraction in EspF translocation. *espF* fused to a β-lactamase (*blaM*) reporter was introduced to the genomes of EPEC-*bfpF* and EPEC-*bfpF* +BfpF^{ara} strains. HeLa cells were infected with these bacterial strains, and their capacity to translocate EspF-BlaM into the host cells was measured by tracking the accumulation of cleaved CCF2, as described (Mills *et al.*, 2008). The time-dependent product accumulation [P] and its derivative [P′] are presented in Figure 2A, top and bottom panels, respectively. The derivative represents the rate by which product molecules (i.e., cleaved CCF2) accumulate in the infected cells. Because CCF2 is present in excess throughout the entire measurement time (Mills *et al.*, 2008), [P′] is proportional to the rate of EspF-BlaM translocation into the cells. Figure 2A clearly shows similar dynamics of [P] accumulation for EPEC-*bfpF* +BfpF^{ara-} and EPEC-*bfpF*. Accumulation of product molecules was negligible following infection with EPEC-*wt* containing the pBAD24 vector. In contrast, upon infection with EPEC-*bfpF* +BfpF$^{ara+(T0)}$, [P] accumulation reached higher levels. This observation is further strengthened by the derivative analysis of [P] (Figure 2A, bottom panel, and Table 1), which revealed two distinct phases of infection. The first occurred between 15 and 30 min infection times, whereby the average [P′] for EPEC-*bfpF* +BfpF^{ara-} and EPEC-*bfpF* (0.37 and 0.56, respectively) was markedly lower than that of EPEC-*bfpF* +BfpF$^{ara+(T0)}$ (1.56). Moreover, the difference between the minimal and maximal [P′] values for EPEC bearing inactivated *bfpF* (~0.6) was small compared with those obtained for the rescued strain (~2.3). These results suggest that, during the early phase of infection, the rate of EspF-BlaM translocation was minimal and nearly steady for

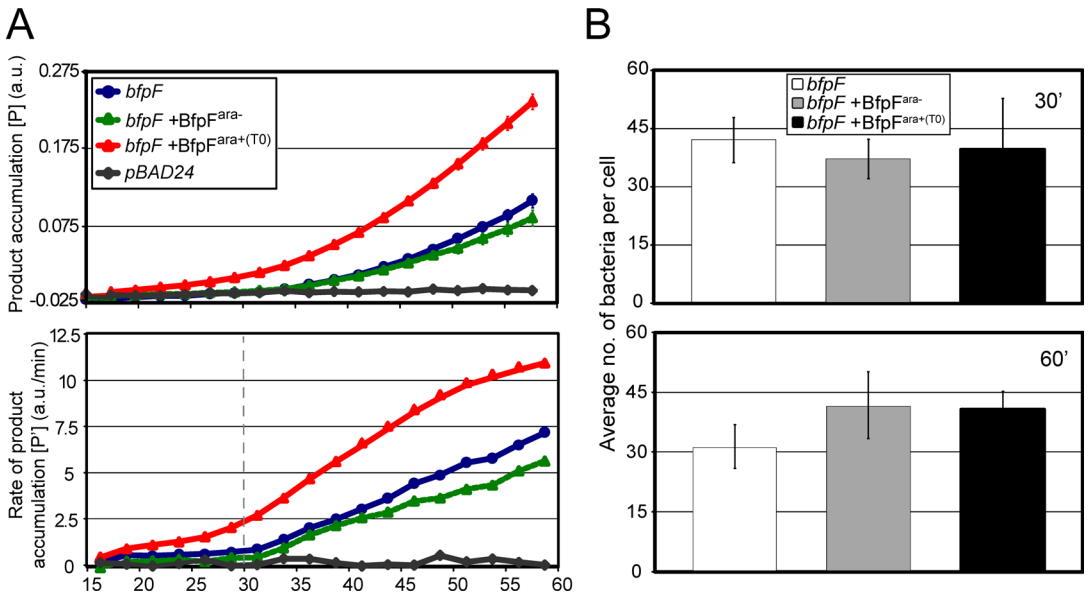

FIGURE 2: BfpF expression is required for efficient translocationof EspF. HeLa cells were infected with the indicated EPEC strains or the pBAD24 vector as control (see *Materials and Methods*). All bacteria expressed the *espF-blaM* reporter gene. (A) Accumulation of cleaved CCF2 [P] (top panel) and its rate of accumulation [P'] (bottom panel) following EPEC infection. HeLa cells were infected with EPEC, and measurement of CCF2 product accumulation was carried out throughout the indicated times. Total product [P] and the rate of its accumulation [P'] were calculated, as explained in *Materials and Methods*. The dashed line in the bottom panel separates the two suggested phases of [P'] as a function of time (see *Results* and Table 1). The results are mean ± SE of four to eight measurements. (B) Levels of EPEC adherence to HeLa cells. HeLa cells were infected with EPEC for 30 or 60 min, and the number of adhered bacteria was determined as described in *Materials and Methods* and Figure S1. Data presented are mean ± SE of three independent experiments.

EPEC-*bfpF* +BfpF^{ara-} and EPEC-*bfpF*. In contrast, the translocation process was faster in the case of EPEC-*bfpF* +BfpF$^{ara+(T0)}$. The second phase was observed between 30 and 60 min of infection, whereby all bacterial strains showed an increase in [P']. The strains unable to express BfpF, however, showed significantly lower [P'] values than those of EPEC-*bfpF* +BfpF$^{ara+(T0)}$, suggesting that the mutant strains had translocated EspF-BlaM at a lower rate than the rescued strain. Importantly, the different EPEC strains colonized the cells at similar levels (Figure 2B). Therefore, the observed differences in translocation rates were not contributed by differences in cell colonization. Translocation data following EPEC-*wt* infection are not shown because high levels of cell detachment were observed after 30 min of infection with this strain (see also Shifrin *et al.*, 2002), posing difficulties in data analysis and interpretation. Altogether, these data implicate BfpF, and its retraction capacity, in the exertion of rapid and competent translocation of EspF and subsequent loss of TJ.

BfpF contributes to efficient assembly of actin-rich pedestals: filamentous (F)-actin staining of fixed cells

The construction of actin-rich pedestals beneath bacterial attachment sites is believed to contribute to bacterial colonization of host cells and is a hallmark of EPEC infection (Campellone and Leong, 2003). To test whether BfpF contributes to the biogenesis of pedestals, MDCK cells were infected with EPEC-*wt* or with EPEC-*bfpF* +BfpF in the absence (ara−) or presence (ara+) of arabinose for 45 and 120 min at 37°C. Bacteria and the actin cytoskeleton were visualized by confocal microscopy following cell staining with DAPI and Texas Red phalloidin, respectively. After 45 min of infection, condensed F-actin staining, which correlated with the DAPI-stained EPEC microcolonies, was broadly visualized in cells infected with EPEC-*wt* or with EPEC-*bfpF* +BfpF$^{ara+(T0)}$ (Figure 3A, arrowheads). In contrast, F-actin staining at infection sites was either invisible (Figure 3A, arrowheads with asterisks) or weak (Figure 3A, arrows) in cells infected with EPEC-*bfpF* +BfpF^{ara-}. After 120 min of cell infection, significant F-actin staining associated with infection sites was seen in all cases. Thus BfpF expression and the subsequent induced pili retraction seem to be important for facilitating F-actin accumulation under EPEC infection sites at early, rather than late, infection times.

Dynamic accumulation of actin and PM fluorescent probes

To further investigate this kinetic effect, we have taken advantage of our recently developed quantitative imaging approach (Sason *et al.*, 2009) to study the effect of BfpF expression on green fluorescent protein (GFP)-actin and monomeric red fluorescent protein (mRFP)-PM accumulation in real time beneath EPEC infection sites. It is of note that the accumulation of GFP-actin fluorescence may represent specific stages in the construction of actin-rich pedestals, whereas the accumulation of mRFP-PM may reflect changes in PM architecture occurring in response to microbe adhesion.

MDCK cells coexpressing GFP-actin and mRFP-PM were infected with EPEC-*wt*, EPEC-*escV*, and EPEC-*bfpF* +BfpF in the absence or presence of arabinose. The fluorescence of GFP-actin (Figure 3B, top) and mRFP-PM (Figure 3B, bottom) at EPEC infection sites was recorded by time-lapse confocal imaging. Infection with EPEC-*wt* resulted in the previously noted profile of GFP-actin accumulation, peaking after ~5 min of EPEC attachment (Sason *et al.*, 2009). In contrast, GFP-actin accumulation under EPEC-*escV* was negligible, confirming that the observed accumulation is T3SS dependent. In the absence of arabinose, EPEC-*bfpF* +BfpF^{ara-} infection resulted in a slight but steady accumulation of GFP-actin, which initiated after ~8 min and leveled off after ~13 min of microcolony attachment. In contrast, when EPEC infection occurred in the presence of arabinose (EPEC-*bfpF* +BfpF$^{ara+(T0)}$), the profile of GFP-actin accumulation was nearly identical to that observed for EPEC-*wt*.

Strain	$t_{15—30}$			$t_{30–60}$		
	Average	Min	Max	Average	Min	Max
EspF-BlaM						
bfpF	0.56	0.17	0.83	4.25	1.37	7.17
bfpF +BfpF^{ara-}	0.37	0	0.57	3.44	1.07	3.77
bfpF +BfpF$^{ara+(T0)}$	1.56	0.57	2.83	7.99	3.77	11.07
Tir-BlaM						
bfpF	5.55	3.41	12.45	43.67	14.76	62.74
bfpF +BfpF^{ara-}	4.67	1.84	9.98	40.46	13.9	63.85
BfpF +BfpF$^{ara+(T0)}$	11.65	3.59	22.57	44.98	27.29	52.67

Values for EspF-BlaM and Tir-BlaM were derived from data presented in Figures 2A and 5, respectively. Values are the average, minimum, and maximum of [P′] at early (15–30 min) and late (30–60 min) phases of EPEC infection.

TABLE 1: Analysis of EspF and Tir-BlaM [P′] in early and late phases of infection.

The mRFP-PM probe accumulated under EPEC-*wt* to a greater extent than EPEC-*escV*, suggesting that some T3SS effectors contribute to its time-dependent accumulation. Infection with EPEC-*bfpF* +BfpF^{ara-} led to minor accumulation of the probe. Addition of arabinose significantly stimulated its accumulation, yet at somewhat lower final levels than EPEC-*wt*. Interestingly, only in cases whereby EPEC expresses BfpF (i.e., EPEC-*wt*, EPEC-*bfpF* +BfpF^{ara+}, and EPEC-*escV*) the early stages (up to ~5 min following microcolony attachment) of mRFP-PM accumulation occurred at similar rates. These early stages may represent initial steps in EPEC association with the host cell surface via BFP attachment and retraction. At later time points, further accumulation of the probe is possibly dependent on subsequent intimate attachments and pedestal formation.

In the experiments described so far, BfpF expression was induced before and during cell exposure to the microbe (T0 condition; see Figure 1). We next tested the ability of arabinose to promote the effects after initial EPEC adherence to the cell surface in the absence of arabinose. Two basic conditions have been applied in these experiments: Either EPEC-*bfpF* +BfpF microcolonies were allowed to interact with the cells in the absence of arabinose during the entire infection time (Figure 3C; EPEC-*bfpF* +BfpF^{ara-}), or the bacteria were first permitted to associate with the cell surface for 15 min in the absence of the inducer and then were exposed to arabinose for the rest of the infection time (Figure 3C**;** EPEC-*bfpF* +BfpF$^{ara+15'}$). In the absence of arabinose, GFP-actin and mRFP-PM accumulated gradually, consistent with the results described earlier in the text (Figure 3B). When bacteria were first adhered in the absence of arabinose and then exposed to the inducer, however, accumulation of both markers was observed ~7 min after induction (Figure 3C). Similar data were obtained in another independent experiment, whereby arabinose was added 2 min following bacterial attachment (Supplemental Figure S3). These results establish a strong temporal relationship between expression of BfpF and actin accumulation following initial adherence of the bacteria to the host cell. Notably again, however, the fact that actin accumulated at similar levels under EPEC-*bfpF* +BfpF^{ara-} and EPEC-*bfpF* +BfpF^{ara+} following longer infection times (e.g., after 16 min; see Figure 3B) suggests that mature actin-rich pedestals may also be formed upon EPEC-*bfpF* +BfpF^{ara-} infection.

Effects on the ultrastructure of infection sites

To determine whether pedestal-like structures are indeed induced in response to BfpF expression, we visualized EPEC- infected apical surfaces by high-resolution transmission electron microscopy following 60 (panels A–D) and 120 min (panels E–H) of infection (Figure 3D). Cells infected with EPEC-*wt* revealed typical pedestal structures (i.e., protrusions of electron-dense and filamentous cytoplasmic staining, likely contributed to by condensed actin filaments beneath intimately attached bacteria). Microvilli effacement at these sites was also observed (panel A). Following 60 min of infection, two types of bacterial interactions with the cell surface were visualized in cells infected with EPEC-*bfpF* +BfpF^{ara-}: In some cases, bacteria were associated with host cell protrusions that resembled pedestals, with little, or sparse electron-dense material (panel B, arrow); in others, bacteria appeared to settle on top of intact microvilli (panel B, arrowheads, and panel C). In contrast, EPEC-*bfpF* +BfpF^{ara+} resided on top of protrusions filled with highly electron-dense branched filament staining (panel D), which were somewhat smaller in size than those observed for EPEC-*wt*. Following 120 min of infection, pedestal structures were observed in all cases (panels E–G), except in cells infected with type III–deficient EPEC-*escV* (panel H).

To summarize, in the absence of arabinose, when BfpF expression is suppressed, bacteria attached to the apical cell surface may form protrusions that contain low levels of condensed actin, possibly representing immature pedestals. Alternatively, bacteria can associate with the apical surface in a way that does not lead to actin condensation beneath them. The latter may reflect their settling on top of intact microvilli without inducing effacement. Yet again, however, these effects seem to be temporal, because following prolonged infection times (e.g., 120 min), pedestals and microvilli effacement appeared to be typical, essentially indistinguishable from those observed for EPEC-*wt*. Thus pedestals can be generated when BfpF expression is suppressed, albeit at a slower pace.

BfpF is required for efficient tyrosine phosphorylation of Tir in polarized epithelial cells

The interaction between Tir and bacteria-associated intimin results in the clustering of Tir-intimin complexes and the subsequent phosphorylation of Tir on two tyrosines located in the C-terminal cytoplasmic region of the protein. One tyrosine, Y474, is the predominant phosphorylation site, the phosphorylation of which prompts the binding of Tir to the adaptor protein Nck and the subsequent recruitment and activation of N-WASP and the Arp2/3 complex. These events eventually lead to actin polymerization and pedestal formation (Campellone and Leong, 2005; Caron *et al.*, 2006). The

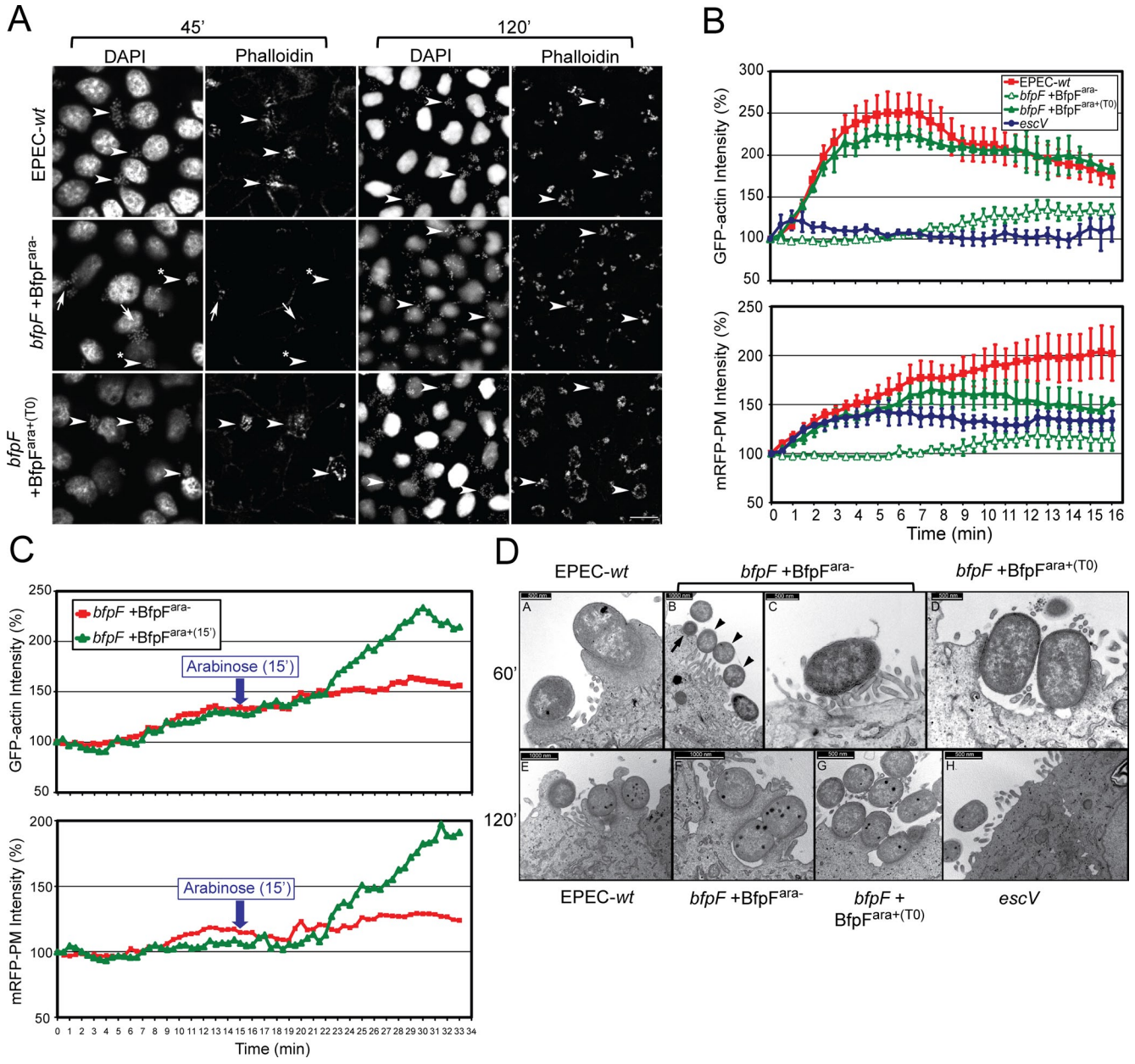

FIGURE 3: Induced BfpF expression is required for efficient production of actin-rich pedestals. (A) Visualization of bacteria and F-actin in fixed cells. MDCK cells were infected with the indicated EPEC strains for 45 and 120 min at 37°C. Cells were fixed and stained with DAPI (bacteria and nuclei) and Texas-Red phalloidin (F- actin). Confocal images were acquired from the apical region of the cells and processed as indicated in *Materials and Methods*. Arrowheads point toward prominent F-actin accumulations associated with EPEC infection sites. Arrows and arrowheads with asterisks indicate weak or barely detectable F-actin accumulations at infection sites, respectively. Bar = 10 μm. (B and C) Quantitative time-lapse imaging analysis of GFP-actin (top panel) and mRFP-PM (bottom panel) accumulation at EPEC infection sites. Cells were cotransfected with plasmids encoding for GFP-actin and mRFP-PM. Cells were subsequently infected under the microscope, and time-lapse live imaging was performed (see Supplemental Movies 6–10). In the case where arabinose-mediated BfpF expression was tested, the inducer was added to the activation medium before cell infection [(EPEC-*bfpF* +BfpF$^{ara+(T0)}$; (B)]; in another experiment, EPEC microcolonies were allowed to interact with the host cell surface for 15 min in medium lacking arabinose, and then the inducer was added until the end of the measurement [(EPEC-*bfpF* +BfpF$^{ara+(T15')}$; (C)]. Fluorescence intensity confined to EPEC attachment sites was quantitatively analyzed. The landing of EPEC microcolonies on the cell surface was identified by differential interference contrast microscopy, and data acquisition started at that time point (designated as time 0). Results presented in panel B are mean ± SE of four experiments. The experiment described in panel C (see Supplemental Movie 10) was repeated, but the microcolony was allowed to interact with the cell surface for 2 min in medium lacking arabinose (Supplemental Figure S3). (D) Ultrastructure of EPEC infection sites. Filter-cultured MDCK cells were infected with the indicated EPEC strains for 60 or 120 min at 37°C. Cells were fixed and processed for observation by transmission electron microscopy, as described in *Materials and Methods*.

second, Y454, is a minor phosphorylation site that plays a lesser role in pedestal biogenesis.

The reduced pedestal observed in EPEC-*bfpF* led us to hypothesize that Tir is either 1) translocated inefficiently or 2) translocated normally but only partially phosphorylated on the critical tyrosines due to other effects, such as ineffective clustering by intimin. To investigate these hypotheses, MDCK cells were infected with EPEC and costained with DAPI (bacteria) and anti-phosphotyrosine (PY) antibodies, which primarily label phosphorylated Tir. Fluorescence images acquired by confocal microscopy and their quantitative analysis are shown in Figure 4, top and bottom panels, respectively. As expected, intense PY staining confined to regions of adherent EPEC-*wt* microcolonies was observed following 45 and 120 min of infection. In contrast, a significantly lower PY signal confined to infection foci was observed in cells infected with EPEC-*bfpF* +BfpF^{ara-} following 45, but not 120, min of infection. Induced BfpF expression (EPEC-*bfpF* +BfpF^{ara+}) resulted in the restoration of intense PY labeling, to levels comparable to those observed for EPEC-*wt*. Infection with EPEC-*escV* did not stimulate the accumulation of the PY signal after 45 or 120 min of infection (unpublished data). From these experiments we learn that BfpF is required for eliciting efficient tyrosine phosphorylation of Tir and that maximal tyrosine phosphorylation of Tir can be achieved in cells infected with EPEC whose BfpF expression is suppressed.

BfpF is required for efficient translocation and tyrosine phosphorylation of Tir

The delay in tyrosine phosphorylation of Tir may be caused by its impaired translocation. To investigate this presumption, the dynamics of Tir-BlaM translocation into HeLa cells following infection with any of the three different EPEC-*bfpF* strains was monitored by tracking the accumulation of the cleaved CCF2 product (Figure 5A, top), and derivative analysis was performed as before (Figure 5A, bottom, and Table 1). The results show that Tir was translocated with similarly slow kinetics by EPEC-*bfpF* or EPEC-*bfpF* +BfpF^{ara-}. In contrast, the translocation rate of Tir was induced upon infection with EPEC-*bfpF* +BfpF^{ara+}. The effect was apparent at early ($t_{15–30}$), but not late ($t_{30–60}$) times of EPEC infection.

To test the efficiency of Tir tyrosine phosphorylation, HeLa cells were infected with EPEC, cell lysates were subjected to immunoprecipitation with anti-PY (4G10) antibodies, and precipitated Tir was identified by its molecular weight using immunoblotting with the same anti-PY antibodies. As expected, tyrosine-phosphorylated Tir (PY-Tir) was detected in cells infected with EPEC-*wt* but not with EPEC-*escV* (Figure 5B) or EPEC that does not express Tir (unpublished data). In cells infected with EPEC-*bfpF* +BfpF^{ara-}, PY-Tir levels were reduced compared with EPEC-*bfpF* +BfpF$^{ara+(T0)}$ or EPEC-*wt*. These data, combined with those presented in Figure 4, reinforce the notion that BfpF expression is needed to elicit efficient translocation and subsequent tyrosine phosphorylation of Tir.

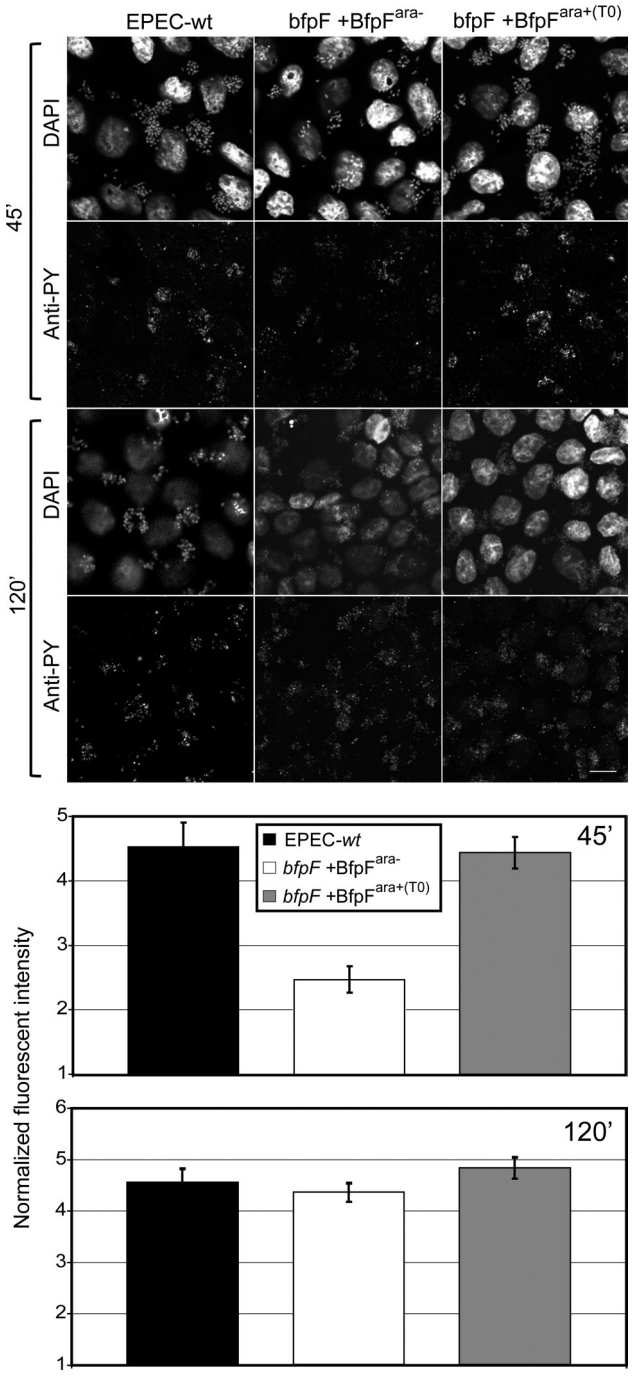

FIGURE 4: BfpF expression is required for efficient tyrosine phosphorylation of Tir in MDCK cells. MDCK cells were infected with EPEC for 45 or 120 min at 37°C. Cells were fixed and stained with DAPI to visualize bacteria and with anti-PY antibodies. Fluorescence was imaged by confocal microscopy, and representative images are shown in the top panel. The intensity of PY fluorescence levels associated with EPEC microcolonies was quantified, and data are presented in the bottom panel. Results are the mean ± SE of at least 20 infection sites imaged in two independent experiments.

DISCUSSION

Retractable Tfp have been shown to be crucial virulence factors, participating in a broad spectrum of fundamental bacterial processes, such as twitching motility, DNA transformation, and early stages of bacterial attachment to host cells (Milgotina, 2009). After mediating initial attachment to the host cell, pili retract. This process is driven by a powerful force-generating machinery that results in the depolymerization of the pilin subunits (>100 pN per retraction of a single pilus, as measured for *N. gonorrhoeae* [Maier *et al.*, 2002]). Similar forces were reported for BFP produced by typical strains of EPEC (Gauthier, 2009). The host cell may sense and respond to these forces by generating a unique platform beneath the adherent bacteria enriched with cortical actin (Merz and So, 2000; Merz *et al.*, 2000), various signal-transducing proteins (Howie *et al.*, 2005, 2008; Lee *et al.*, 2005), and proteins of the junctional/polarity complex (Coureuil *et al.*, 2009). Despite accumulating knowledge, however,

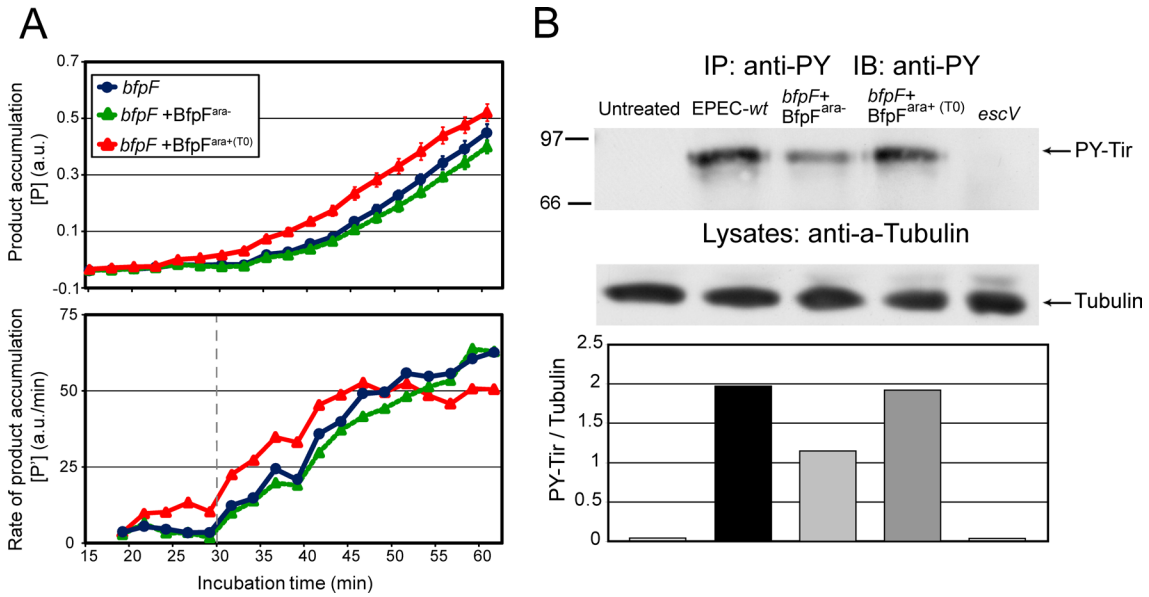

FIGURE 5: BfpF expression is essential for efficient translocation and tyrosine phosphorylation of Tir in HeLa cells. (A) Tir translocation. HeLa cells were infected with EPEC-*bfpF*, EPEC-*bfpF* +BfpF^{ara-}, and EPEC-*bfpF* +BfpF$^{ara+(T0)}$ expressing the *tir-blaM* reporter gene. Experiments were carried out and analyzed as indicated in *Materials and Methods* and Figure 2A. The results are mean ± SE of four to eight measurements. (B) Tir phosphorylation. HeLa cells were infected with the indicated EPEC strains or left untreated. Cells were lysed and subjected to immunoprecipitation (IP) with anti-PY antibodies followed by SDS–PAGE and immunoblotting (IB) with the same antibodies. PY-Tir is indicated with an arrow (top panel). Cell lysates were probed with anti–α-tubulin antibodies (middle panel, indicated with an arrow). Densitometric analysis was performed, and the PY-Tir/Tubulin ratio is shown (bottom panel). The results are representative of three independent experiments.

little is known about how these host cell responses are translated to pathogenic effects.

Earlier studies have shown that the EPEC-*bfpF* mutant and EPEC-*wt* display comparable attaching and effacing phenotypes (Anantha *et al.*, 1998). In this study, we used an inducible expression system and a variety of sensitive dynamic assays to show that BfpF is required for efficient translocation of EPEC effectors, construction of actin-rich pedestals, and the breakdown of TJs. As these effects are hallmarks of EPEC pathogenesis, our data may explain previous in vivo studies, demonstrating that the ability of a *bfpF* mutant to cause disease is attenuated in a human experimental model (Bieber *et al.*, 1998).

How does BFP retraction elicit the observed host-cell responses? We propose the following model, which links pili dynamics with effector translocation and host cell responses to infection (Figure 6). In the absence of pili retraction, we presume that bacteria are hyperpiliated (Figure 6A). The excessive and long pili hinder the close contact between the bacterial and host cell surfaces. Thus these surfaces are separated by a large space that precludes efficient insertion of the T3SS injectisome and, subsequently, the bacterial effectors into the host cell. Ineffective EspF translocation (Figure 2A), and possibly of other TJ disrupting effectors (for a review, see Guttman and Finlay, 2009), may contribute to the loss of bacterial ability to break down the TJ barrier (Figure 1) and to the attenuated EPEC disease (Bieber *et al.*, 1998). Ineffective Tir translocation could have caused reduced tyrosine phosphorylation levels on host cell–inserted Tir (Figures 4 and 5B) and the consequent slower development of actin-rich pedestals (Figure 3). Interestingly, whereas the EspF translocation rate was reduced throughout the entire infection time, the rate of Tir translocation was lower only at earlier phases ($t_{15–30}$) of EPEC-*bfpF* infection (see Table 1). The greater effect on EspF could be explained by the observation that Tir is translocated more efficiently than EspF into cells infected with EPEC-*wt* (Mills *et al.*, 2008).

Bundlin subunits expressed by the typical EPEC strain bind *N*-acetyllactoseamine in vitro and in cells, and this association can plausibly induce BFP retraction (Hyland *et al.*, 2008; Humphries *et al.*, 2009, 2010). Pili retraction by this or any other mechanism, would promptly and effectively close the gap between the bacterial and the host cell surfaces. This action would facilitate efficient T3SS-dependent translocation of bacterial effectors across the host cell PM and into the host cells (Figure 6B), resulting in effective disruption of TJs, high tyrosine phosphorylation levels of Tir, and competent construction of actin-rich pedestals. A study that concurs with our hypothesis reveals that the length of *Yersinia pestis* surface-adhesin YadA, which binds to a host cell surface receptor, determines the efficiency with which the bacteria inject their effectors into the host cell cytoplasm (Mota *et al.*, 2005).

EPEC seems to generate a specialized protein and lipid domain at the bacterium-host cell interaction site. This domain resembles a gigantic lipid raft enriched with cholesterol (Allen-Vercoe *et al.*, 2006), phosphoinositides (PIs; Sason *et al.*, 2009; Campellone, 2010; Saarikangas *et al.*, 2010), caveolin (Boettcher *et al.*, 2010), and elements of the actin cytoskeleton (Caron *et al.*, 2006). It is interesting to note in this context that PI3-kinase, its downstream effectors PI(3,4,5)P_3, and Akt have been shown to be concentrated beneath *N. gonorrhoeae* infection sites. Interestingly, the PI has been shown to be translocated to the outer leaflet of the PM and to be active in stimulating the expression of PilT (an orthologue of EPEC BfpF), pili retraction, and microcolony growth (Lee *et al.*, 2005). Similar processes may also be relevant for EPEC infection, as we have recently shown that EPEC can simulate the recruitment of PI3-kinase and PI(3,4,5)P_3 beneath its infection site (Sason *et al.*, 2009). It is possible that during retraction the pili expose hidden

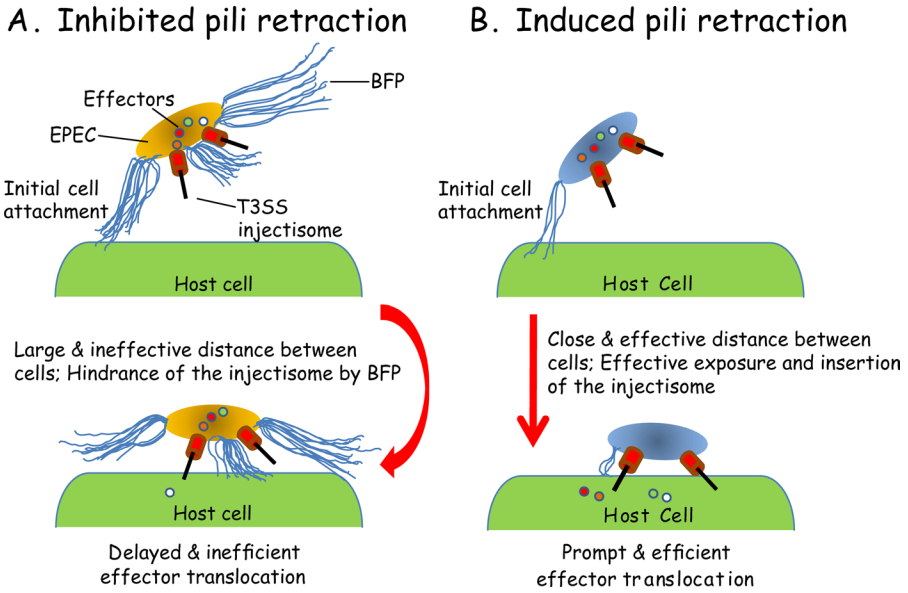

FIGURE 6: A working model linking pili retraction with the effectiveness of bacterial effector translocation. The model is described in the *Discussion* section.

epitopes (Biais *et al.*, 2010) that interact with specific lipids and proteins associated with the host cell PM. Another possibility is that BFP retraction brings other bacterial surface components (adhesins) to contact the host cell surface and modulate the nearby membrane environment. A third scenario suggests that modulation of PM organization is generated in response to mechanical forces exerted by the retracting pili on the host cell. This hypothesis is principally supported by findings showing that mechanical forces artificially imposed on the cells, mimicking the forces generated by Tfp retraction, stimulate mechanosensitive signaling pathways in the cells (Howie *et al.*, 2005). We predict that deciphering the molecular basis underlying these pilus-stimulated, mechanosensitive pathways in the host cell will lay the groundwork for the development of novel antibacterial drugs aimed at combatting a broad range of Tfp-producing microorganisms.

Although the foregoing considerations apply to typical EPEC strains that express BFP, it is worth noting that in recent years the contribution of atypical strains that do not express BFP to human disease has been increasingly appreciated (Trabulsi *et al.*, 2002). Whether and by what mechanism such strains achieve efficient effector delivery and equivalent virulence in the absence of pilus retraction, or are simply less virulent than typical EPEC strains, remain questions for further investigation.

MATERIALS AND METHODS

Bacterial strains and plasmids

EPEC strains used in this study are listed in Supplemental Table S1. UMD946 (referred to herein as EPEC-*bfpF*) is a derivative of the wild-type EPEC strain E2348/69, in which the Walker A box was replaced with a scar sequence (unpublished data). Walker box motifs are required for ATP hydrolysis and, in the case of Tfp systems, are presumed to energize the extrusion and retraction of the pilus filament. Thus this alteration of BfpF is expected to produce pili that cannot retract, yielding bacteria considered to be hyperpiliated. EPEC-*bfpF* bacteria complemented with a plasmid encoding for intact BfpF are predicted to have restored BFP retraction capacity, and therefore to be phenotypically similar to the wild-type strain. In this study, EPEC-*bfpF* complemented with a plasmid (pJAL-F1) containing an intact *bfpF* gene under the control of an arabinose-inducible promoter was generated as follows. The *bfpF* gene was amplified from pRPA102 (Anantha *et al.*, 1998) using primers Infusion bfpF Fwd: (5′-TAGCAGGAGGAATTCGGGAA-TTCCTGATTCGGTGTGATATCATG-3′) and Infusion bfpF Rev: (5′-GCAGGTCGACTCTA-GAGGTCTAGATGCCATAATATTT-TAGCTAATCAGGTT-3′), Platinum *Pfx* polymerase (Invitrogen, San Diego, CA) and 25 cycles of denaturation (95°C for 1 min), annealing (58°C for 1 min), and elongation (68°C for 1 min). The gel-purified PCR product was spliced using the In Fusion method (Clontech, Mountain View, CA) into pBAD24 previously digested with *Eco*RI and *Xba*I, downstream of the *pBAD24 arabinose* promoter, and transformed into *E. coli* XL 10-Gold cells (Agilent Technologies, Santa Clara, CA). The resulting plasmid, pJAL-F1, was confirmed by digestion with *Eco*RI and *Xba*I, which yielded the expected fragment of ~1-kb base pair and by sequencing with pBAD-Fwd and pBAD-Rev standard primers. The pJAL-F1 plasmid was then transformed into the *bfpF* mutant strain, UMD946. We refer herein to UMD946 complemented with the arabinose-responsive pJAL-F1 plasmid as EPEC-*bfpF* +BfpF^{ara}.

Cells

MDCK cells were cultured as described (Sason *et al.*, 2009). We used the Caco-2BBe Tet-off clone (Shen *et al.*, 2006) as a model for polarized human enterocytes, which morphologically and functionally resemble the enterocytes lining the small intestine (Hidalgo *et al.*, 1989). Cells were routinely maintained in DMEM supplemented with 10% (vol/vol) fetal calf serum (FCS), L-glutamine, nonessential amino acids, and antibiotics (Biological Industries, Beit-Ha'Emek, Israel). Approximately 50,000 cells were seeded on a 12-mm Transwell support (Corning, Acton, MA) precoated with rat-tail collagen and grown for 19–25 d before EPEC infection, as described (Turner *et al.*, 1997). HeLa cells were cultured routinely in DMEM supplemented with 10% FCS and antibiotics.

Induction of BfpF expression

Expression of BfpF was suppressed when EPEC-*bfpF* +BfpF^{ara} was incubated in medium lacking arabinose (EPEC-*bfpF* +BfpF^{ara-}); under these conditions pilus retraction is inhibited. Addition of arabinose (0.2% wt/vol; EPEC-*bfpF* +BfpF^{ara+}) stimulates BfpF expression, and so the presumed capacity of pili retraction. Evidence for these phenotypes is provided by time-lapse imaging of bacterial disaggregation in solution (performed as in Anantha *et al.*, 1998, and Supplemental Figure S4A), and EPEC microcolony merging on the cell surface of infected cells, as described (Supplemental Figure S4B; Supplemental Movies 1–5). Addition of arabinose had no effect on any of the examined parameters in cells infected with EPEC strains that do not harbor pJAL-F1 (unpublished data).

Bacterial activation and cell infection

Bacterial activation and cell infection were performed essentially as described (Sason *et al.*, 2009). Briefly, bacteria cultured for 18 h at

37°C in Luria-Bertani medium were diluted 1:50 (vol/vol) into MEM-Eagle with Hanks salts (for infection of MDCK cells) or into DMEM (for infection of Caco-2 and HeLa cells), and were incubated for 3 h at 37°C and 5% CO_2 without shaking to induce expression of *bfp* and LEE genes. Cells were infected with preactivated bacteria at a multiplicity of infection of ~100. Infection was carried out in activation medium supplemented with 5% FCS (for MDCK cells) or 10% FCS (for Caco-2 and HeLa cells) at 37°C and 5% CO_2.

Monitoring the barrier functions of TJs

TER and FITC-dextran permeability measurements of polarized MDCK or Caco-2 cell monolayers were performed as described (Sason *et al.*, 2009). Briefly, the apical poles of the cells were infected with 0.5 ml of preactivated bacteria supplemented with FCS and 2 mg/ml of 4 kDa FITC-dextran. Prewarmed medium (1.5 ml) with FCS was added to the basolateral chamber. Cells were incubated in 5% CO_2, 37°C, and 97% humidity. TER was measured using the Millicell-ERS system (Millipore, Bedford, MA) equipped with a silver/silver-chloride electrode. Measurements were performed hourly and at 37°C. The value of a blank Transwell filter (with no cells, but otherwise treated identically) was subtracted from the resistance values of filter-cultured cells. Typical TER values recorded before cell infection (i.e., at time zero) were 90–100 and 160–200 Ωcm^2 for MDCK and Caco-2BBe cell monolayers, respectively. The fluorescence intensity of a 100 µl aliquot taken from the basolateral medium was measured in a BMG Galaxy Fluostar microplate reader (BMG Lab Instruments, Offenburg, Germany) equipped with a 485/538 nm excitation/emission filter pair.

Transmission electron microscopy

EPEC-infected cell monolayers were fixed, postfixed, dehydrated, embedded in epoxy resin, thin sectioned, and viewed as described (Orzech *et al.*, 2000) with minor modifications. Fixation and postfixation reagents were dissolved in 0.1 M cacodylate buffer, pH 7.0. The resin used for infiltration and embedding was Agar-100 (Agar Scientific, Stansted, Essex, England). Images were captured on a Tecnai 12 electron microscope (FEI, Phillips, Eindhoven, The Netherlands) equipped with MegaView 2 CCD camera and AnalySIS 3.0 software (Soft Imaging System, Münster, Germany).

Indirect immunofluorescence and confocal microscopy

Immunofluorescence labeling of MDCK cells was carried out as described (Sason *et al.*, 2009). Briefly, cells were washed three times in phosphate-buffered saline (PBS) and fixed with 4% paraformaldehyde. Following extensive washes, cells were permeabilized, washed with PBS, and incubated with blocking solution (0.025% [wt/vol] saponin, 0.6% [wt/vol] fish skin gelatin in PBS) for 15 min at 37°C. Following washes, cells were incubated with primary antibodies (see Table S2) in blocking solution for 1 h at 37°C. Cells were then washed five times in blocking solution with rigorous shaking for 10 min each, and incubated with appropriate secondary antibodies (Table S2) for 1 h at 37°C. Cells were postfixed with paraformaldehyde. F-actin labeling was performed by incubating permeabilized cells with 0.5 U/ml Texas-Red Phalloidin (Invitrogen) in blocking solution for 15 min at 22°C. Bacteria and cell nuclei were labeled with DAPI (100 ng/ml in PBS) for 1 min at 22°C. Cells were mounted and visualized using an upright Leica TCS SP5 laser-scanning confocal microscope, equipped with 63×, NA 1.4 oil lens (Leica, Wetzlar, Germany). Confocal XY sections were taken at *z*-axis intervals of 0.5 µm. Wavelengths of excitation lasers and spectral emission bands are indicated in Table S3. Image processing was done with ImageJ (http://rsbweb.nih.gov/ij/) and Adobe Photoshop 7.0 (Adobe Systems).

Quantitative analysis of fluorescently immunolabeled phosphotyrosine beneath attached EPEC

MDCK cells were first infected with EPEC and then costained with DAPI, to visualize cell-associated bacterial microcolonies, and with anti-PY mAb 4G10 followed by appropriate secondary antibodies. The latter identifies phosphorylated tyrosine labeling, contributed to mainly by tyrosine phosphorylation of PM-incorporated Tir. Cells were fixed, and confocal images were acquired as mentioned earlier in text. Quantitative image analysis of the PY signal beneath attached EPEC was performed as follows: Confocal sections, in which the microcolony-associated PY signal was maximal, were projected using the "averaged Z-projection" ImageJ macro. The average fluorescence intensity of regions encompassing membrane-associated EPEC microcolonies was measured and normalized to regions not occupied by bacteria. Data are the average of at least 20 measurements performed in two independent experiments.

Biochemical detection of PY-Tir

HeLa cells cultured on a 10-cm plate were infected with EPEC for 45 min at 37°C. Cells were washed with ice-cold (4°C) PBS and lysed for 5 min at 4°C with 150 µl of lysis buffer (20 mM TrisCl, pH 7.2, 150 mM NaCl, 5 mM EDTA, 1% wt/vol NP-40, 10% wt/vol glycerol) containing phosphatase inhibitors (2 mM Na_3VO_4, 1 mM NaF, 2 mM Na_4PO_7) and 1 mM phenylmethylsulfonyl fluoride. Cell lysates were then centrifuged (5 min, 3000 × *g*, 4°C) and a 100 µl fraction of the supernatant was subjected to immunoprecipitation, using anti-PY mAb 4G10 bound to protein G-Sepharose beads (GE Healthcare, Uppsala, Sweden) for 1 h at 4°C. After washing the beads with ice-cold lysis buffer and PBS, the resulting immunocomplexes were analyzed by SDS–PAGE and Western blotting and subsequently probed with anti-PY (4G10) antibodies. Cell lysates were probed with anti-α tubulin antibodies. Protein bands were visualized by the EZ-ECL chemiluminescence assay kit (Biological Industries). Consistent with previous reports (Rosenshine *et al.*, 1996; Kenny *et al.*, 1997), PY-Tir was identified as a major band of ~90 kDa.

Time-lapse imaging of live cells

Experiments were carried out essentially as described (Sason *et al.*, 2009). Briefly, MDCK cells grown on glass-bottom plates (MatTek, Ashland, MA) were cotransfected with plasmids encoding GFP-actin and an mRFP-PM. The mRFP-PM (provided by S. Grinstein, Hospital for Sick Children, Toronto, ON, Canada) consists of mRFP fused to the N-terminal 11 amino acids of the Src-family kinase Lyn that is both myristoylated and doubly palmitoylated. These lipid moieties target the construct to the inner leaflet of the PM, mainly to lipid rafts (Sason *et al.*, 2009). Protein expression was allowed for 40–48 h. EPEC infection was performed under the confocal microscope (37°C, 5% CO_2, and 97% humidity). Cell imaging and quantitative image analyses were carried out as described (Sason *et al.*, 2009). Wavelengths of excitation lasers and narrow-band emission filters are listed in Supplemental Table S3.

Real-time analysis of EspF- and Tir- BlaM translocation

The procedure was carried out as described (Mills *et al.*, 2008). Briefly, EPEC strains were separately conjugated with pCX446 (*espF::blaM*) and pCX442 (*tir::blaM*) by crossing with *E. coli* SM10 harboring the appropriate plasmid. Integration of the fusion genes into the EPEC chromosome was verified by PCR with primers

5′-GGCTGTATGGATGATGAGTC-3′ (forward) and 5′-GATAATACCGCGCCACATAG-3′ (reverse) for *espF::blaM* and 5′- GTTGGGTACCATGTTTAGTCCAACGGCAATGG-3′ (forward) and 5′-GATAATACCGCGCCACATAG-3′ (reverse) for *tir::blaM*. Measurement of effector translocation is based on BlaM activity in infected HeLa cells. To insure that extracellular BlaM activity does not falsely contribute to the signal, experiments were performed in the presence of 0.45 μM BlaM inhibitor protein, which inhibits extracellular BlaM. We used EPEC-*wt* containing the pBAD24 vector as a negative control. Levels of BlaM activity product [P] were obtained, and the rate of product accumulation [P′], which is proportional to the levels of effector-BlaM, was derived using the following expression:

$$[P']_{\frac{t(n)+t(n+1)}{2}} = \frac{[P_{t(n+1)}]-[P_{t(n)}]}{t_{(n+1)}-t_{(n)}}$$

Presented [P′] values are moving averages along three time points. The number of cell-adhered bacteria was determined as described in Figure 2B.

Statistical analysis

Results are presented as means ± SE. Statistical significance was determined by two-tailed Student's *t* test. A p value < 0.05 indicates a statistically significant difference.

ACKNOWLEDGMENTS

This work was supported by the Israel Science Foundation (B.A., I.R), Public Health Service award R01 AI-37606 (to M.S.D.) from the National Institutes of Health (NIH), and NIH Grant T32 GM008181 (to J.A.L.).

REFERENCES

Allen-Vercoe E, Waddell B, Livingstone S, Deans J, DeVinney R (2006). Enteropathogenic Escherichia coli Tir translocation and pedestal formation requires membrane cholesterol in the absence of bundle-forming pili. Cell Microbiol 8, 613–624.

Anantha RP, Stone KD, Donnenberg MS (1998). Role of BfpF, a member of the PilT family of putative nucleotide-binding proteins, in type IV pilus biogenesis and in interactions between enteropathogenic Escherichia coli and host cells. Infect Immun 66, 122–131.

Biais N, Higashi DL, Brujic J, So M, Sheetz MP (2010). Force-dependent polymorphism in type IV pili reveals hidden epitopes. Proc Natl Acad Sci USA 107, 11358–11363.

Bieber D, Ramer SW, Wu CY, Murray WJ, Tobe T, Fernandez R, Schoolnik GK (1998). Type IV pili, transient bacterial aggregates, and virulence of enteropathogenic Escherichia coli. Science 280, 2114–2118.

Boettcher JP, Kirchner M, Churin Y, Kaushansky A, Pompaiah M, Thorn H, Brinkmann V, Macbeath G, Meyer TF (2010). Tyrosine-phosphorylated caveolin-1 blocks bacterial uptake by inducing Vav2-RhoA-mediated cytoskeletal rearrangements. PLoS Biol 8, 8e1000457.

Campellone KG (2010). Phosphoinositides influence pathogen surfing: EPEC rights the SHIP. Cell Host Microbe 7, 1–2.

Campellone KG, Leong JM (2003). Tails of two Tirs: actin pedestal formation by enteropathogenic E. coli and enterohemorrhagic E. coli O157:H7. Curr Opin Microbiol 6, 82–90.

Campellone KG, Leong JM (2005). Nck-independent actin assembly is mediated by two phosphorylated tyrosines within enteropathogenic Escherichia coli Tir. Mol Microbiol 56, 416–432.

Caron E, Crepin VF, Simpson N, Knutton S, Garmendia J, Frankel G (2006). Subversion of actin dynamics by EPEC and EHEC. Curr Opin Microbiol 9, 40–45.

Chen HD, Frankel G (2005). Enteropathogenic Escherichia coli: unravelling pathogenesis. FEMS Microbiol Rev 29, 83–98.

Coureuil M *et al.* (2009). Meningococcal type IV pili recruit the polarity complex to cross the brain endothelium. Science 325, 83–87.

Donnenberg MS, Calderwood SB, Donohue-Rolfe A, Keusch GT, Kaper JB (1990). Construction and analysis of TnphoA mutants of enteropathogenic Escherichia coli unable to invade HEp-2 cells. Infect Immun 58, 1565–1571.

Donnenberg MS, Giron JA, Nataro JP, Kaper JB (1992). A plasmid-encoded type IV fimbrial gene of enteropathogenic Escherichia coli associated with localized adherence. Mol Microbiol 6, 3427–3437.

Gauthier NC (2009). Bundle-forming pili from enteropathogenic *Escherichia coli* generate moderate forces. Biophys J 96, 519a.

Giron JA, Donnenberg MS, Martin WC, Jarvis KG, Kaper JB (1993). Distribution of the bundle-forming pilus structural gene (bfpA) among enteropathogenic Escherichia coli. J Infect Dis 168, 1037–1041.

Guttman JA, Finlay BB (2008). Subcellular alterations that lead to diarrhea during bacterial pathogenesis. Trends Microbiol 16, 535–542.

Guttman JA, Finlay BB (2009). Tight junctions as targets of infectious agents. Biochim Biophys Acta 1788, 832–841.

Guttman JA, Li Y, Wickham ME, Deng W, Vogl AW, Finlay BB (2006). Attaching and effacing pathogen-induced tight junction disruption in vivo. Cell Microbiol 8, 634–645.

Hidalgo IJ, Raub TJ, Borchardt RT (1989). Characterization of the human colon carcinoma cell line (Caco-2) as a model system for intestinal epithelial permeability. Gastroenterology 96, 736–749.

Howie HL, Glogauer M, So M (2005). The N. gonorrhoeae type IV pilus stimulates mechanosensitive pathways and cytoprotection through a pilT-dependent mechanism. PLoS Biol 3, e100.

Howie HL, Shiflett SL, So M (2008). Extracellular signal-regulated kinase activation by Neisseria gonorrhoeae downregulates epithelial cell proapoptotic proteins Bad and Bim. Infect Immun 76, 2715–2721.

Humphries RM, Donnenberg MS, Strecker J, Kitova E, Klassen JS, Cui L, Griener TP, Mulvey GL, Armstrong GD (2009). From alpha to beta: identification of amino acids required for the N-acetyllactosamine-specific lectin-like activity of bundlin. Mol Microbiol 72, 859–868.

Humphries RM, Griener TP, Vogt SL, Mulvey GL, Raivio T, Donnenberg MS, Kitov PI, Surette M, Armstrong GD (2010). N-acetyllactosamine-induced retraction of bundle-forming pili regulates virulence-associated gene expression in enteropathogenic Escherichia coli. Mol Microbiol 76, 1111–1126.

Hyland RM, Sun J, Griener TP, Mulvey GL, Klassen JS, Donnenberg MS, Armstrong GD (2008). The bundlin pilin protein of enteropathogenic Escherichia coli is an N-acetyllactosamine-specific lectin. Cell Microbiol 10, 177–187.

Iguchi A *et al.* (2009). Complete genome sequence and comparative genome analysis of enteropathogenic Escherichia coli O127:H6 strain E2348/69. J Bacteriol 191, 347–354.

Jerse AE, Yu J, Tall BD, Kaper JB (1990). A genetic locus of enteropathogenic Escherichia coli necessary for the production of attaching and effacing lesions on tissue culture cells. Proc Natl Acad Sci USA 87, 7839–7843.

Kenny B, DeVinney R, Stein M, Reinscheid DJ, Frey EA, Finlay BB (1997). Enteropathogenic E. coli (EPEC) transfers its receptor for intimate adherence into mammalian cells. Cell 91, 511–520.

Kline KA, Falker S, Dahlberg S, Normark S, Henriques-Normark B (2009). Bacterial adhesins in host-microbe interactions. Cell Host Microbe 5, 580–592.

Lee SW, Higashi DL, Snyder A, Merz AJ, Potter L, So M (2005). PilT is required for PI(3,4,5)P3-mediated cross-talk between Neisseria gonorrhoeae and epithelial cells. Cell Microbiol 7, 1271–1284.

Maier B, Potter L, So M, Long CD, Seifert HS, Sheetz MP (2002). Single pilus motor forces exceed 100 pN. Proc Natl Acad Sci USA 99, 16012–16017.

Marcos LA, DuPont HL (2007). Advances in defining etiology and new therapeutic approaches in acute diarrhea. J Infect 55, 385–393.

McNamara BP, Koutsouris A, O'Connell CB, Nougayrede JP, Donnenberg MS, Hecht G (2001). Translocated EspF protein from enteropathogenic Escherichia coli disrupts host intestinal barrier function. J Clin Invest 107, 621–629.

Merz AJ, So M (2000). Interactions of pathogenic neisseriae with epithelial cell membranes. Annu Rev Cell Dev Biol 16, 423–457.

Merz AJ, So M, Sheetz MP (2000). Pilus retraction powers bacterial twitching motility. Nature 407, 98–102.

Milgotina EDM (2009). The bundlin-forming pilus and other Type IV pili. In: Pili and Flagella: Current Research and Future Trends, ed. KF Jarrell, Norfolk (UK): Caister Academic Press.

Mills E, Baruch K, Charpentier X, Kobi S, Rosenshine I (2008). Real-time analysis of effector translocation by the type III secretion system of enteropathogenic Escherichia coli. Cell Host Microbe 3, 104–113.

Mota LJ, Journet L, Sorg I, Agrain C, Cornelis GR (2005). Bacterial injectisomes: needle length does matter. Science 307, 1278.

Nataro JP, Kaper JB (1998). Diarrheagenic Escherichia coli. Clin Microbiol Rev 11, 142–201.

Orzech E, Cohen S, Weiss A, Aroeti B (2000). Interactions between the exocytic and endocytic pathways in polarized Madin-Darby canine kidney cells. J Biol Chem 275, 15207–15219.
Philpott DJ, McKay DM, Sherman PM, Perdue MH (1996). Infection of T84 cells with enteropathogenic Escherichia coli alters barrier and transport functions. Am J Physiol 270, G634–G645.
Rosenshine I, Ruschkowski S, Stein M, Reinscheid DJ, Mills SD, Finlay BB (1996). A pathogenic bacterium triggers epithelial signals to form a functional bacterial receptor that mediates actin pseudopod formation. EMBO J 15, 2613–2624.
Rothbaum R, McAdams AJ, Giannella R, Partin JC (1982). A clinicopathologic study of enterocyte-adherent Escherichia coli: a cause of protracted diarrhea in infants. Gastroenterology 83, 441–454.
Rothbaum RJ, Partin JC, Saalfield K, McAdams AJ (1983). An ultrastructural study of enteropathogenic Escherichia coli infection in human infants. Ultrastruct Pathol 4, 291–304.
Saarikangas J, Zhao H, Lappalainen P (2010). Regulation of the actin cytoskeleton-plasma membrane interplay by phosphoinositides. Physiol Rev 90, 259–289.
Sason H, Milgrom M, Weiss AM, Melamed-Book N, Balla T, Grinstein S, Backert S, Rosenshine I, Aroeti B (2009). Enteropathogenic Escherichia coli subverts phosphatidylinositol 4,5-bisphosphate and phosphatidylinositol 3,4,5-trisphosphate upon epithelial cell infection. Mol Biol Cell 20, 544–555.
Shen L, Black ED, Witkowski ED, Lencer WI, Guerriero V, Schneeberger EE, Turner JR (2006). Myosin light chain phosphorylation regulates barrier function by remodeling tight junction structure. J Cell Sci 119, 2095–2106.
Shifrin Y, Kirschner J, Geiger B, Rosenshine I (2002). Enteropathogenic Escherichia coli induces modification of the focal adhesions of infected host cells. Cell Microbiol 4, 235–243.
Simonovic I, Rosenberg J, Koutsouris A, Hecht G (2000). Enteropathogenic Escherichia coli dephosphorylates and dissociates occludin from intestinal epithelial tight junctions. Cell Microbiol 2, 305–315.
Taylor CJ, Hart A, Batt RM, McDougall C, McLean L (1986). Ultrastructural and biochemical changes in human jejunal mucosa associated with enteropathogenic Escherichia coli (0111) infection. J Pediatr Gastroenterol Nutr 5, 70–73.
Taylor DN, Echeverria P (1993). Diarrhoeal disease: current concepts and future challenges. Molecular biological approaches to the epidemiology of diarrhoeal diseases in developing countries. Trans R Soc Trop Med Hyg 87, Suppl 33–5.
Trabulsi LR, Keller R, Tardelli Gomes TA (2002). Typical and atypical enteropathogenic Escherichia coli. Emerg Infect Dis 8, 508–513.
Turner JR, Rill BK, Carlson SL, Carnes D, Kerner R, Mrsny RJ, Madara JL (1997). Physiological regulation of epithelial tight junctions is associated with myosin light-chain phosphorylation. Am J Physiol 273, C1378–C1385.